

Effects of onshore and offshore environmental parameters on the leading edge erosion of wind turbine blades

A comparative study

Shankar Verma, Amrit; Jiang, Zhiyu; Ren, Zhengru; Hu, Weifei; Teuwen, Julie J.E.

DOI

[10.1115/1.4049248](https://doi.org/10.1115/1.4049248)

Publication date

2021

Document Version

Final published version

Published in

Journal of Offshore Mechanics and Arctic Engineering

Citation (APA)

Shankar Verma, A., Jiang, Z., Ren, Z., Hu, W., & Teuwen, J. J. E. (2021). Effects of onshore and offshore environmental parameters on the leading edge erosion of wind turbine blades: A comparative study. *Journal of Offshore Mechanics and Arctic Engineering*, 143(4), Article 042001. <https://doi.org/10.1115/1.4049248>

Important note

To cite this publication, please use the final published version (if applicable).
Please check the document version above.

Copyright

Other than for strictly personal use, it is not permitted to download, forward or distribute the text or part of it, without the consent of the author(s) and/or copyright holder(s), unless the work is under an open content license such as Creative Commons.

Takedown policy

Please contact us and provide details if you believe this document breaches copyrights.
We will remove access to the work immediately and investigate your claim.

Effects of onshore and offshore environmental parameters on the leading edge erosion of wind turbine blades: A comparative study

Amrit Shankar Verma ^{*1}, Zhiyu Jiang², Zhengru Ren³, Weifei Hu⁴ and Julie J.E. Teuwen¹

¹Faculty of Aerospace Engineering, Delft University of Technology (TU Delft), The Netherlands

² Department of Engineering Sciences, University of Agder, Grimstad, Norway

³Department of Marine Technology, Norwegian University of Science and Technology (NTNU), Trondheim, Norway

⁴School of Mechanical Engineering, Zhejiang University, Hangzhou, China

Abstract

The presence of rain-induced leading edge erosion of wind turbine blades necessitates the development of erosion models. One of the essential parameters for erosion modelling is the relative impact velocity between rain droplets and the rotating blade. Based on this parameter, the erosion damage rate of a wind turbine blade is calculated to estimate the expected leading edge lifetime. The environmental conditions that govern this parameter have site-specific variations, and thus, rain and wind loading on a turbine differ for onshore and offshore locations. In addition, there are wave loads present in the offshore environment. The present paper tries to provide guidelines for erosion modelling and investigates whether there are differences in erosion of blades due to (1) varying rainfall conditions modelled using different droplet size distributions for onshore and offshore locations in combination with (2) winds of varying turbulence intensities and (3) wave-induced loads. Aero-hydro-servo-elastic simulations are carried out for an onshore wind turbine and a monopile-supported offshore wind turbine. Furthermore, erosion variables such as the relative impact velocities and the associated erosion damage rate of a blade are analysed for various blade azimuth angles. The study shows that the rainfall intensity and turbulence intensity minorly influence the impact velocity and pressure but have a substantial effect on the overall erosion damage rate. Additionally, a significantly higher erosion damage rate is found for blades exposed to offshore rainfall conditions than for blades under onshore rainfall conditions. Furthermore, no substantial influence on erosion is found because of wave-induced loads.

* Corresponding author. Email address: a.s.verma@tudelft.nl

INTRODUCTION

1 The consistent demand for the reduction of carbon footprint in the energy sector has motivated power
2 production from sustainable sources such as wind, hydro, wave and solar power sources [1]. Among the
3 different resources, wind energy is one of the most reliable and readily available power sources and can be
4 harnessed using wind turbines (WTs) [2, 3] (Figure 1(a)). Given that the power extracted from the WT
5 increases with the rotor swept area along with the cube of the wind speed, large WTs are currently in
6 high demand both in onshore and offshore sectors [4, 5]. Another major advantage that drives the design
7 of large-sized WTs is the reduced operation and maintenance costs [6]. This upscaling in the size of WTs
8 is profitable. However, it poses several engineering challenges. For instance, latest generation of wind
9 turbine blades (WTBs) rotate with tip speeds in the range of 60-120 m/s and are exposed to high velocity
10 impact with rain droplets during precipitation. The recurring high velocity impacts between rain droplets
11 and rotating blades during their service life exert cyclic fatigue stresses on the WTBs. This eventually
12 leads to the leading edge erosion (LEE) of WTBs that includes development of pitting and surface cracks
13 at the leading edge (Figure 1(b)). In severe cases, the damage could even penetrate into the composite
14 substrate (Figure 1(b)) [7, 8].

15 LEE of a WTB is a critical issue to the wind turbine performance. LEE causes the local roughening
16 of surfaces, which in turn provokes the premature transition of laminar flow into turbulent flow along
17 the leading edge, thereby reducing the aerodynamic efficiency and annual energy production (*AEP*) of
18 a turbine [9]. In general, regular inspection, maintenance and repair of WTBs due to LEE is inevitable
19 to keep up with the target *AEP* of a turbine through the design life, thereby increasing the cost of
20 wind energy. It has been reported by [9, 10] that repair and maintenance due to LEE costs the European
21 offshore wind turbine sector more than £56 million annually. Therefore, LEE of WTBs requires immediate
22 attention.

23 Several research efforts are being made to address the issue of LEE due to high velocity rain droplet
24 impact. These include developing, testing and comparing leading edge coating systems in accelerated
25 rain erosion tests and quantifying their rain erosion resistance in excess of 100-200 m/s droplet impact
26 [14, 15, 16]. Another aspect for controlling rain erosion of a WTB is to develop a control algorithm
27 [17], which automatically reduces the tip speed of the blade (and thus the impact velocity) in the event
28 of harsh precipitation, thereby inhibiting cumulative fatigue damage accumulation due to repeated rain
29 droplet impact. Computational models [7, 18] are also being developed where emphasis is on estimating

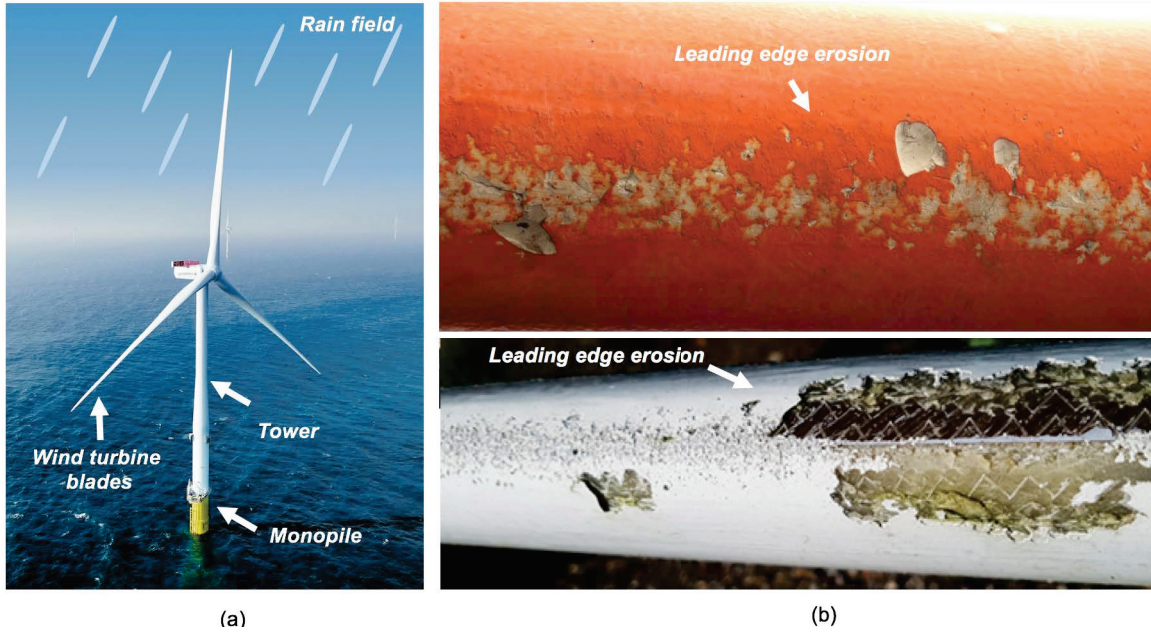


Figure 1: (a) Wind turbine exposed to rain field [Modified picture from source: Vattenfall group[11]] (b) Leading edge erosion of wind turbine blades [12, 13][Source: TNO and DURALEEDGE project]

30 the fatigue life based on cyclic stresses induced on the leading edge over its service life.

31 Amirzadeh et al. [19] developed a computational framework to estimate the fatigue life of a blade,
 32 where erosion damage rates for the leading edge under varying impact velocities and different rainfall
 33 conditions were evaluated. Similar studies can also be found in [15, 20, 21, 22], where fluid structure
 34 interaction models are developed using sophisticated numerical codes. However, one of the simplifications
 35 in all the previous studies is that a maximum impact velocity between 100-140 m/s is simply assumed for
 36 analysis purposes, and the effects of droplet impact angles, blade surface curvature, varying wind speeds
 37 and blade rotation are ignored. In principle, for the fatigue design of the coating material, it is essential
 38 to quantify the impact velocity and cyclic variation during blade rotation as well as their dependence on
 39 the rainfall intensity, droplet impact angle and wind condition to which a WTB is exposed. It has been
 40 shown in the literature [8, 16, 23] that the erosion damage rate (\dot{D}_i) of the leading edge modelled as a
 41 flat surface is proportional to the 6.7th power of the impact velocity ($|\vec{V}_{imp}|^{6.7}$). Therefore, this makes the
 42 relative impact velocity between rain droplets and the rotating blade an essential parameter for erosion
 43 modelling and damage prediction of the leading edge of the wind turbine blade.

44 The environmental conditions that govern the above mentioned erosion parameters have site-specific
 45 variations, and thus, rain and wind loading on a turbine differ for onshore and offshore locations. For
 46 instance, less turbulent winds are present in the offshore environment together with rainfall having varying
 47 statistical characteristics at onshore and offshore locations [25]. In addition, there are wave loads present

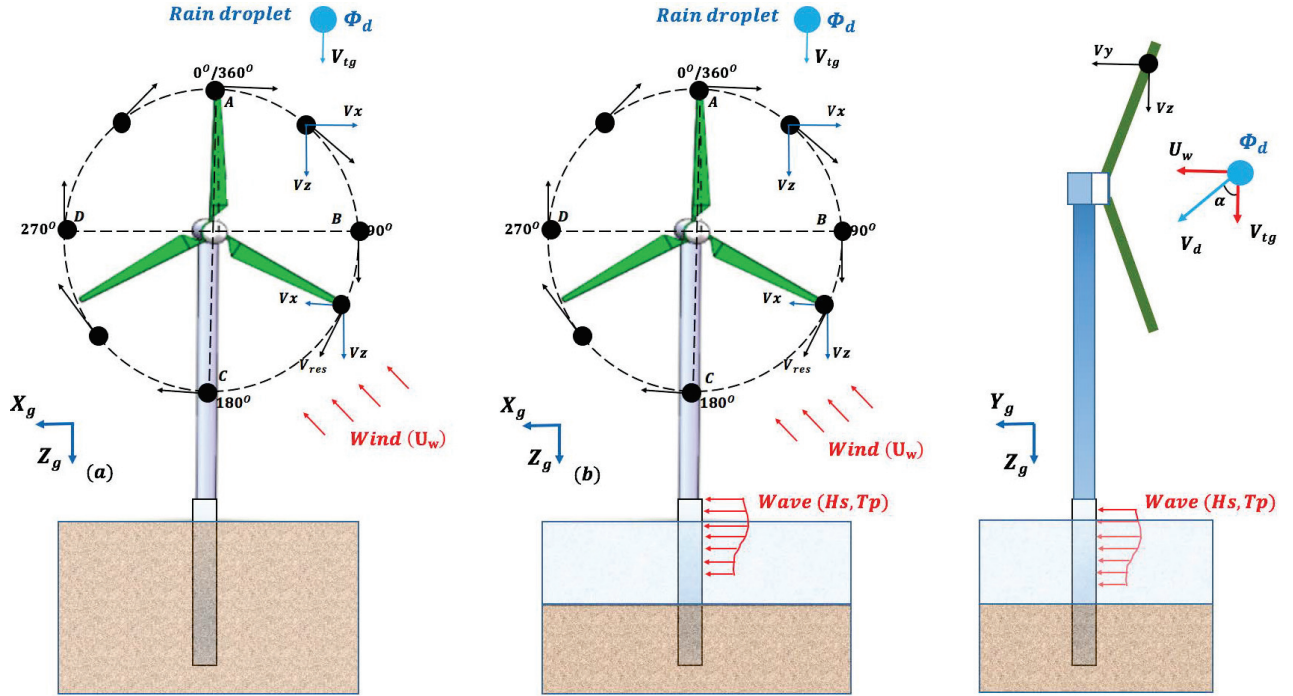


Figure 2: Different input variables related to onshore and offshore wind turbines (Modified figure from [24]) and definition of impact angle α

48 in the offshore environment (Figure 2) that can cause additional dynamic responses in the WT and can
 49 affect the overall erosion damage rate of WTBs. Thus, the present paper tries to provide guidelines for
 50 erosion modelling and investigates whether there are differences in erosion of blades due to (1) varying
 51 rainfall conditions modelled using different droplet size distributions for onshore and offshore locations
 52 in combination with (2) winds of varying turbulence intensities and (3) wave-induced loads. The aim of
 53 the paper is to provide guidelines on whether all these parameters need to be included for site-specific
 54 LEE modelling. For this purpose, aero-hydro-servo-elastic simulations are carried out for an onshore
 55 wind turbine and a monopile-supported offshore wind turbine, both having similar turbine settings of an
 56 NREL 5 MW open-source wind turbine. Realistic environmental conditions are modelled separately for
 57 both onshore and offshore locations and erosion variables such as the impact velocities and the associated
 58 erosion damage rate of a blade are analysed. In addition, an assessment is presented at varying blade
 59 azimuth angles. The next section describes in detail the problem definition and the analysis procedure.

60 PROBLEM DEFINITION AND ANALYSIS PROCEDURE

61 There are two main erosion parameters that are of interest in this paper for studying the effects of
 62 environmental parameters on the erosion of onshore and offshore WTBs. These parameters include -

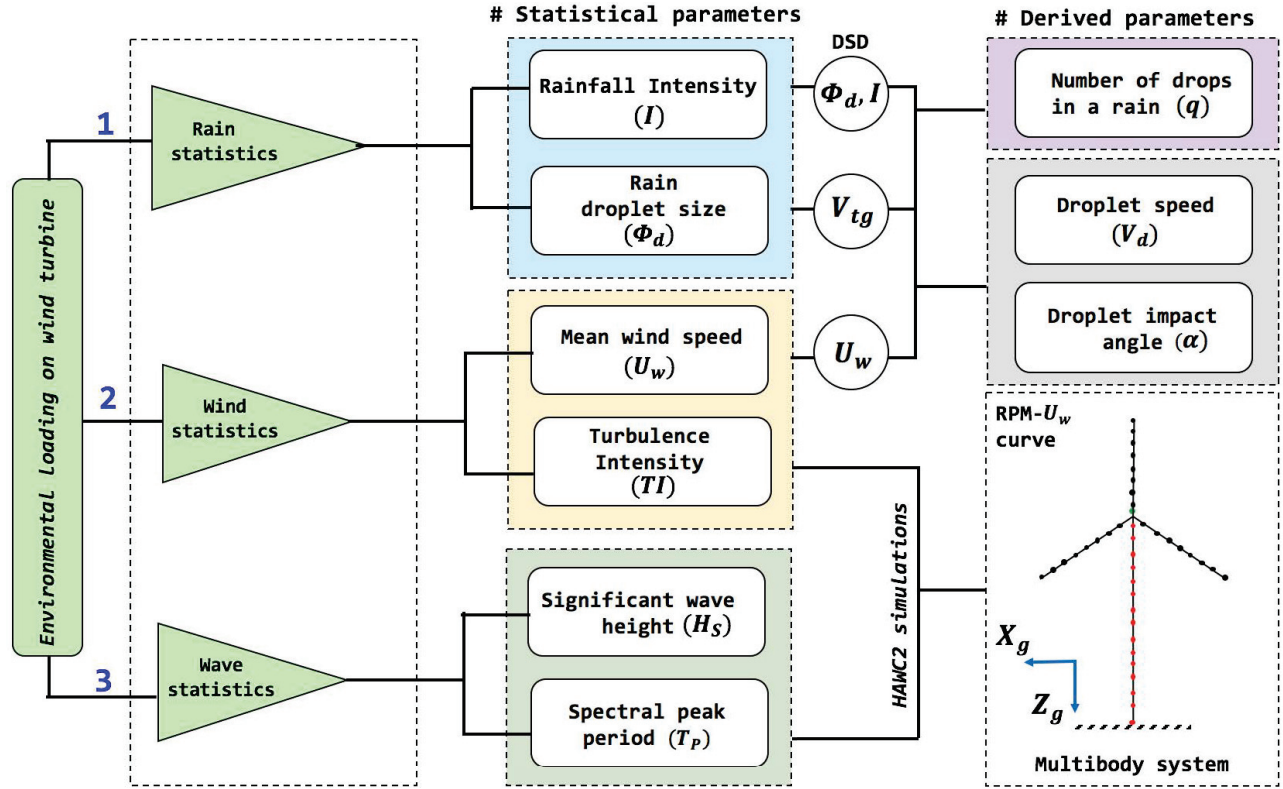


Figure 3: Flowchart showing different source of environmental loads on wind turbine and associated statistical parameters

63 (a) the relative impact velocity between rain droplets and rotating blades (\vec{V}_{imp}), and (b) the associated
64 erosion damage rate of the rotating blade contributed from the repetitive impact with the rain droplets
65 (\dot{D}_i). Principally, these parameters depend primarily on the statistics of the environmental conditions
66 to which a wind turbine is exposed during its service life (see Figure 3). The parameters are described
67 through (1) rain statistics that are defined by two statistical parameters - the rainfall intensity (I), which
68 is defined as the total accumulated rainfall in a given period of time expressed in $mm/hour$, and rain
69 droplet size (ϕ_d), which represents the diameter of rain droplets in a given rain. Furthermore, (2) wind
70 statistics are described by the mean wind speed (U_w) and turbulence intensity (TI), and (3) wave statistics
71 are described based on the significant wave height (H_s) and wave spectral peak period (T_p). Figure 3 also
72 shows other parameters that are derived from the rain and wind statistics and are essential for erosion
73 modelling, such as the number of drops for a given instance of rain (q), the droplet speed (V_d) and the
74 droplet impact angle (α). The discussions about how these parameters are calculated in this paper are
75 mentioned in the subsequent sections. In addition, it is also essential to define the steady state rotor
76 speed-wind speed curve of the wind turbine that decides the tip speed of the blade for a given wind speed.
77 Note that for a given wind turbine and as a result of these statistical parameters, \vec{V}_{imp} is expected to vary

78 with the blade azimuth angle ($\theta \in [0^\circ, 360^\circ]$) and different radial positions (r) along the blade length (l).

79 **I. Relative impact velocity between rain droplets and the rotating blade (\vec{V}_{imp})**

80 The relative impact speed between a falling rain droplet and a rotating blade can be expressed as follows
81 (see the velocity triangle in Figure 2):

$$|\vec{V}_{imp}| = \sqrt{(V_x)^2 + (V_y - V_d \sin\alpha)^2 + (V_z - V_d \cos\alpha)^2} \quad (1)$$

82 where V_x , V_y , and V_z are the absolute velocity components of the blade in the global frame X_g , Y_g and
83 Z_g directions and V_d is the assumed droplet speed in the same frame. V_d is defined as (Figure 2) [26]:

$$V_d = \sqrt{U_w^2 + V_{tg}^2} \quad (2)$$

84 α is defined as the droplet impact angle and is defined as [26] (see Figure 2):

$$\alpha = \arctan\left(\frac{U_w}{V_{tg}}\right) \quad (3)$$

85 where V_{tg} is defined as the vertical terminal speed of a rain droplet, and its magnitude is given by:

$$V_{tg} = 9.65 - 10.3e^{-0.6\phi_d} \quad (0.5mm < \phi_d < 5mm) \quad (4)$$

86 Note that in the above equations, U_w is the horizontal mean wind speed and is considered the component
87 of the rain droplet velocity in the Y_g direction. On the other hand, V_{tg} is defined as the vertical
88 terminal speed of a rain droplet and is considered the component of the rain droplet velocity in the
89 Z_g direction. This is considered for simplicity; nevertheless, the actual droplet impact angle and droplet
90 velocity components may deviate because of the influence of the rotating blades on the induced velocities.

91 A list of assumptions that are considered in Eqs. (1) to (4) are summarised below:

92 (1) The axial and circumferential inductions of the air flow are ignored for the estimation of the droplet
93 velocity and it is approximated as the sum of the free stream wind velocity (U_w) and the terminal velocity
94 (V_{tg}).

95 (2) Wind turbine blade is modelled as a rotating line body (1D geometry) and the surface is modelled
96 as flat while computing erosion damage rate. Also, the impact angle described through Eq. (3) neglects
97 the effects of the blade surface curvature.

98 (3) The local transport and trajectory deviation of raindrops due to the aerodynamic field around the

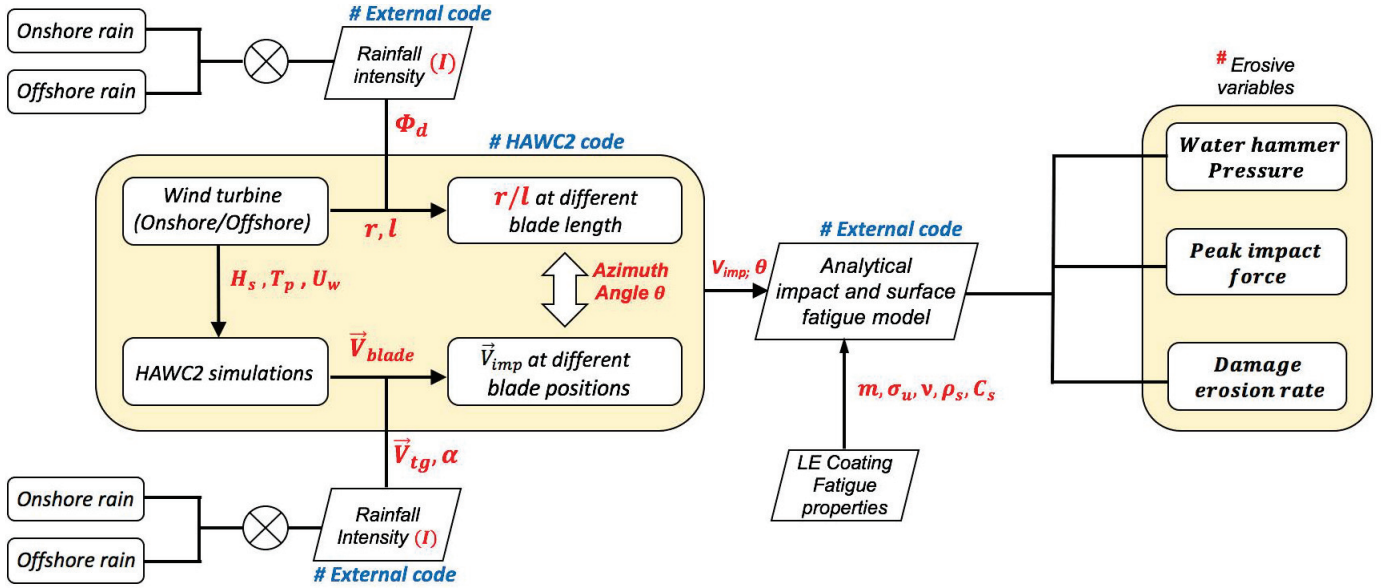


Figure 4: Analysis procedure considered in the study

99 blade section is neglected.

100 Droplet size distribution (DSD): Onshore and offshore rainfall

101 There exists a probabilistic distribution of droplet diameter (ϕ_d) in a given rain, which is related to the
 102 rainfall intensity (I) through a droplet size distribution (DSD). In general, this distribution varies for
 103 onshore and offshore rainfall conditions. The rainfall scenario for the onshore condition is defined using
 104 Best's distribution, which is given by [27]:

$$F(\phi_d) = 1 - \exp \left[- \left(\frac{\phi_d}{1.3I^{0.232}} \right)^{2.25} \right] \quad (5)$$

105 Similarly, for representing the rainfall scenario for the offshore conditions, the DSD is given by [25]:

$$F(\phi_d) = 1 - \exp \left[- \left(\frac{\phi_d}{1.03I^{0.138}} \right)^{2.83I^{-0.0953}} \right] \quad (6)$$

106 where $F(\phi_d)$ is the cumulative distribution function (CDF) of the droplet size. In Eqs. (5) and (6) above,
 107 the droplet diameter ϕ_d is expressed in mm, whereas I is expressed in mm/hr . Note that the offshore
 108 DSD, shown in Eq. (6), was recently developed by Herring et al. [25], where a CDF for ϕ_d based on one
 109 year of measured data was derived for offshore conditions and compared with the estimates from Best's
 110 DSD [27]. Notable differences were found between the distributions with droplet sizes overestimated using
 111 Best's DSD [27]. However, it should be noted that the data for analysis in [25] for offshore conditions are

112 based on only one year of recorded data and require further improvement. Therefore, in this study, Best's
 113 distribution [27] is used to represent rainfall scenarios at both onshore and offshore locations for all cases,
 114 and a representative droplet size is selected for different I . However, a standalone comparative study is
 115 performed in this paper to exclusively check the effect of varying DSDs for onshore and offshore conditions
 116 on the LEE of WTBs. Note that the use of these DSDs includes a few assumptions; for instance, droplets
 117 are assumed to be spherical for all cases, and the effects of changes in the shape of the droplets, especially
 118 for higher rainfall intensities, are neglected.

119 All the variables discussed through these equations are also marked in a flow chart shown in Figure
 120 4, where the analysis framework of the study is described. First, aero-hydro-servo-elastic simulations are
 121 carried out in HAWC2 [28] for a rotating blade based on the NREL 5 MW turbine [29] by considering
 122 realistic environmental conditions for land-based WT and monopile-supported offshore wind turbine.
 123 From the analysis, the rotational speed of the blade is evaluated at different θ along the blade span
 124 length (r/l). Furthermore, these results are combined with an in-house external code describing rainfall
 125 parameters ϕ_d , I , α and V_{tg} , and $|\vec{V}_{imp}|$ is estimated using Eq. (1). The details of the environmental load
 126 cases considered in this study are described in the next section. Once $|\vec{V}_{imp}|$ is evaluated, the structural
 127 responses of the leading edge due to rain droplet impact are evaluated using different erosion variables
 128 and are discussed below.

129 II. Peak impact forces, impact pressure and associated LEE damage rate (\dot{D}_i)

130 The following are the LE structural response parameters that are used to quantify LEE damage: (a) peak
 131 impact forces (F_{imp}), (b) water hammer pressure (p_{wh}), and (c) erosion damage rate (D_i) (Figure 4). The
 132 F_{imp} on the blade's leading edge is given by an analytical model developed by [30, 31]. The analytical
 133 model is verified in our previous work for wind turbine blades [20], and F_{imp} is given as:

$$F_{imp} = 0.84 \rho_w |\vec{V}_{imp}|^2 \phi_d^2 \quad (7)$$

134 where ρ_w is the density of water taken as 1000 kg/m^3 . Furthermore, the erosion damage rate is defined
 135 by an analytical surface fatigue damage model developed and validated by [8, 16]. The model applies
 136 Miner's rule to estimate \dot{D}_i and is given by:

$$\dot{D}_i = \frac{\dot{N}}{N_{ic}} = \frac{q |\vec{V}_{imp}| \beta_d}{8.9 \left(\frac{S}{\phi_d^2 p_{wh}} \right)^{5.7}} \quad (8)$$

137 where $\dot{D}_i \geq 1$ represents fatigue damage and q is the number of droplets per unit volume of rainfall, which
 138 is given by:

$$q = 530.5 \frac{I}{V_{tg} \phi_d^3} \quad (9)$$

139 where I is defined in mm/hr , ϕ_d is defined in mm , and V_{tg} is defined in m/s . It should be noted that the
 140 above equation for q corresponds to the ideal rainfall conditions where it is assumed that all the droplets
 141 in an event of rain have a size equal to the median droplet diameter that is estimated from a given DSD
 142 and rain intensity (I). β_d is the impingement efficiency given by the relation:

$$\beta_d = 1 - e^{-15\phi_d} \quad (10)$$

143 p_{wh} is the water hammer pressure defined by:

$$p_{wh} = \frac{\rho_w c_w |\vec{V}_{imp}|}{1 + \frac{\rho_w c_w}{\rho_s c_s}} \quad (11)$$

144 where ρ_s and c_s are the density and speed of sound in the coating material, respectively. S is the erosive
 145 strength of the coating material defined by:

$$S = \frac{4\sigma_u(m-1)}{1-2\nu} \quad (12)$$

146 where σ_u , m and ν are the ultimate strength, Wöhler slope and Poisson's ratio of the coating material,
 147 respectively. In this study, a polyethylene terephthalate (PET)-based thermoplastic coating material [14]
 148 is used to determine the erosion damage rate. The material properties are tabulated in Table 1.

Table 1: Material properties for coating material [14]

Parameter	Values	Units
ρ_s	1320	kg/m ³
c_s	2480	m/s
σ_u	57.6	MPa
m	14.9	-
ν	0.395	-

149 **MATERIAL AND MODELLING METHOD**

150 A generic 5 MW-based wind turbine originally designed by NREL is modelled in aeroelastic HAWC2 code
 151 [28] for estimating the global motion responses of the rotating blade for both onshore and offshore wind
 152 turbines. The code is based on multibody dynamics where structural systems can be discretised with
 153 timoshenko beam elements and components of the turbine can be connected together through constraints
 154 or joints. The code is able to simulate time domain responses of wind turbines under the action of
 155 aerodynamic and hydrodynamic loads. The design parameters for the NREL 5 MW wind turbine are
 156 provided in Table 2.

157 Figure 5 presents the numerical model for the offshore wind turbine considered in the study, where the
 158 NREL 5 MW turbine [29] is adapted based on the phase II model of Offshore Code Comparison (OC3)
 [32]. Realistic soil properties are defined for the monopile, having a diameter of 9 m. An eigenfrequency

Table 2: Description of NREL 5-MW reference turbine [29]

Rating	5MW turbine
Rotor orientation, configuration	Upwind, 3 Blades
Control Variable speed	Collective pitch
Drive train High speed	Multiple-stage gearbox
Rotor, Hub diameter	126 m, 3 m
Hub height	90 m
Cut-in, Rated, Cut-out wind speed	3 m/s, 11.4 m/s, 25 m/s
Cut-in, Rated rotor speed	6.9 rpm, 12.1 rpm
Rated tip speed	80 m/s
Rotor mass	110,000 kg
Nacelle mass	240,000 kg
Tower mass	347,460 kg

159 analysis is performed for the offshore WT, and the natural period in the first fore-aft and side-side bending
 160 modes is found to be approximately 4.2 s (T_{FA} , $T_{SS} = 4.2s$). It should be noted that in the original
 161 OC3 model, the damping ratio of the first fore-aft and side-side bending mode of the turbine is close to
 162 0.2%, which is tuned to a value of 1% critical in this study as per recommendations and experimental
 163 observations from [33]. The structural components, including blades, monopiles and towers, are modelled
 164 using timoshenko beam elements, and the soil is defined through distributed springs. The hydrodynamic
 165

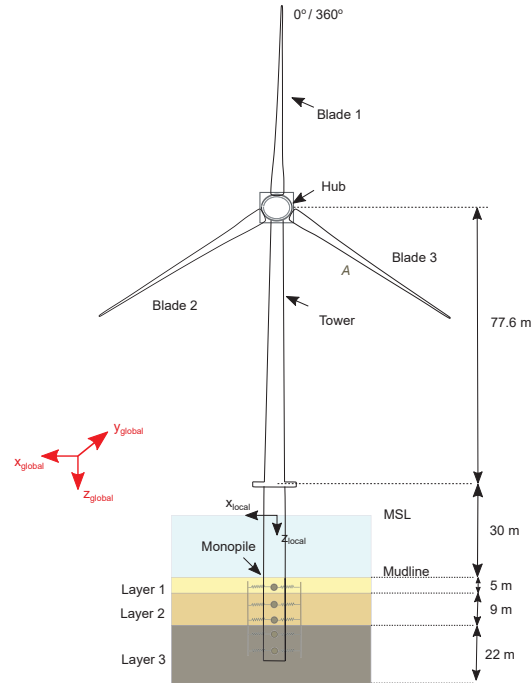


Figure 5: Numerical model considered in HAWC2 for offshore wind turbine

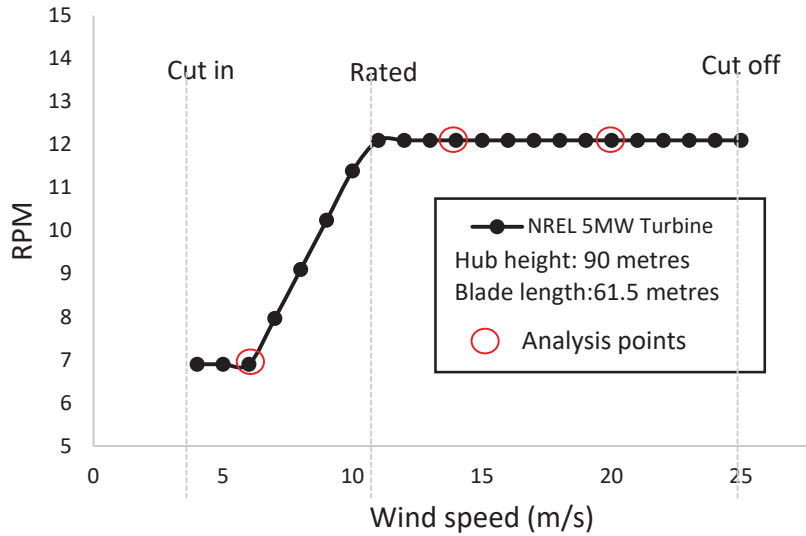


Figure 6: Rotor speed-mean wind speed curve for the NREL 5MW wind turbine

166 loads on the monopile are calculated by Morison's equation[34], and the JONSWAP spectrum[35] is used
 167 to generate the irregular waves. Furthermore, in HAWC2 simulations [36], aerodynamic loads on the blade
 168 are evaluated using Blade Element Momentum (BEM) theory with engineering corrections. The BEM
 169 implemented in HAWC2 includes several engineering models, such as dynamic inflow (dynamic induction),
 170 skew inflow, dynamic stall and the near-wake model. The efficiency of these models in HAWC2 is validated
 171 against the CFD and the advanced vortex model for blade loads and axial induction; see [37, 38]. However,

172 BEM cannot account for advanced flow effects such as wake rotation and hence may affect the local flow
 173 phenomenon, but the corrected BEM is still useful for engineering aeroelastic analysis. Furthermore,
 174 inflow wind turbulence is generated using Mann's turbulence box [39] in the HAWC2 code, and the effects
 175 of wind shear are included. The details of the parameters used for generating the turbulence can be found
 176 in another work [2, 40]. Additionally, the model for the onshore wind turbine is similar to the offshore
 177 wind turbine except that (1) the tower of the land-based turbine is rigidly connected at the bottom and
 (2) there are no hydrodynamic loads acting on the turbine.

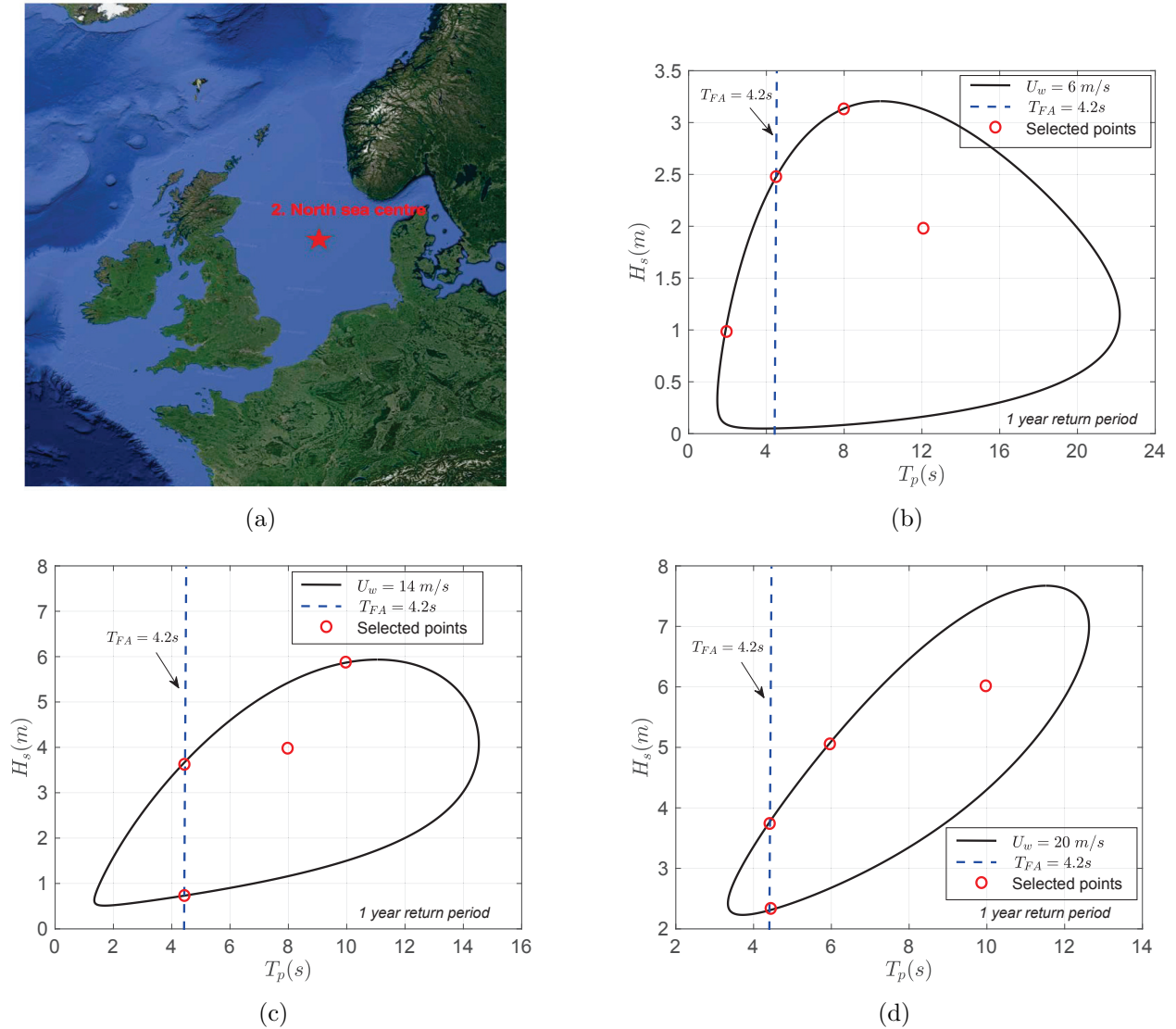


Figure 7: (a) North sea centre offshore site; 2D contour surface for H_s , T_p for (b) $U_w=6\text{m/s}$ (c) $U_w=14\text{m/s}$ (d) $U_w=20\text{m/s}$ and selected load cases

Table 3: Load cases considered for the analysis

EC	U_w (m/s)	TI	H_s (m)	T_p (s)
EC1	6	0, 0.06, 0.12, 0.26	1.00	2.00
EC2	6	0, 0.06, 0.12, 0.26	2.30	4.20
EC3	6	0, 0.06, 0.12, 0.26	3.14	8.00
EC4	6	0, 0.06, 0.12, 0.26	2.00	12.00
EC5	14	0, 0.06, 0.12, 0.26	0.70	4.20
EC6	14	0, 0.06, 0.12, 0.26	3.50	4.20
EC7	14	0, 0.06, 0.12, 0.26	4.00	8.00
EC8	14	0, 0.06, 0.12, 0.26	6.00	10.00
EC9	20	0, 0.06, 0.12, 0.26	2.27	4.20
EC10	20	0, 0.06, 0.12, 0.26	4.90	4.20
EC11	20	0, 0.06, 0.12, 0.26	5.00	6.00
EC12	20	0, 0.06, 0.12, 0.26	6.00	10.00

179 **Environmental load cases**

180 **Wave and wind conditions:**

181 To analyse LEE subjected to rain droplet impact for both onshore and offshore wind turbines, three
182 different mean wind speeds, i.e., $U_w = 6, 14, 20$ m/s, are considered in this study. These cases range
183 between the cut-in and rated wind (Figure 6) speed of a turbine ($U_w = 6$ m/s), the rated and cut-off
184 speed ($U_w = 14$ m/s), and a speed that is closer to the cut-off speed ($U_w = 20$ m/s). Furthermore, for each
185 case of U_w , four different turbulence intensities (TI) are considered ($TI = 0, 0.06, 0.12, 0.26$). These
186 values represent steady wind and wind with low, medium and high turbulence, respectively. For instance,
187 $TI = 0.06$ represents the turbulence level at which the offshore wind turbine operates, while $TI = 0.26$
188 corresponds to inflow wind conditions during gusts and storms.

189 To consider the effect of wave-induced loads on the offshore wind turbine, the North Sea centre is
190 considered as a representative offshore site (Figure 7(a)), and the 2D contour surface [3] for different
191 combinations of significant wave heights (H_s) and wave spectral peak periods (T_p) for a chosen U_w are
192 shown in Figures 7(b)-(d). The red dots in Figures 7(b)-(d) correspond to the selected load cases for
193 the offshore wind turbine. Note that the points where the vertical line intersects the contour surface
194 correspond to the case close to the highest resonance frequency of the turbine ($T_{FA} = 4.2$ s). Overall,
195 twelve load cases (EC1 to EC12) are considered and given in Table 3. Additionally, for each load case,

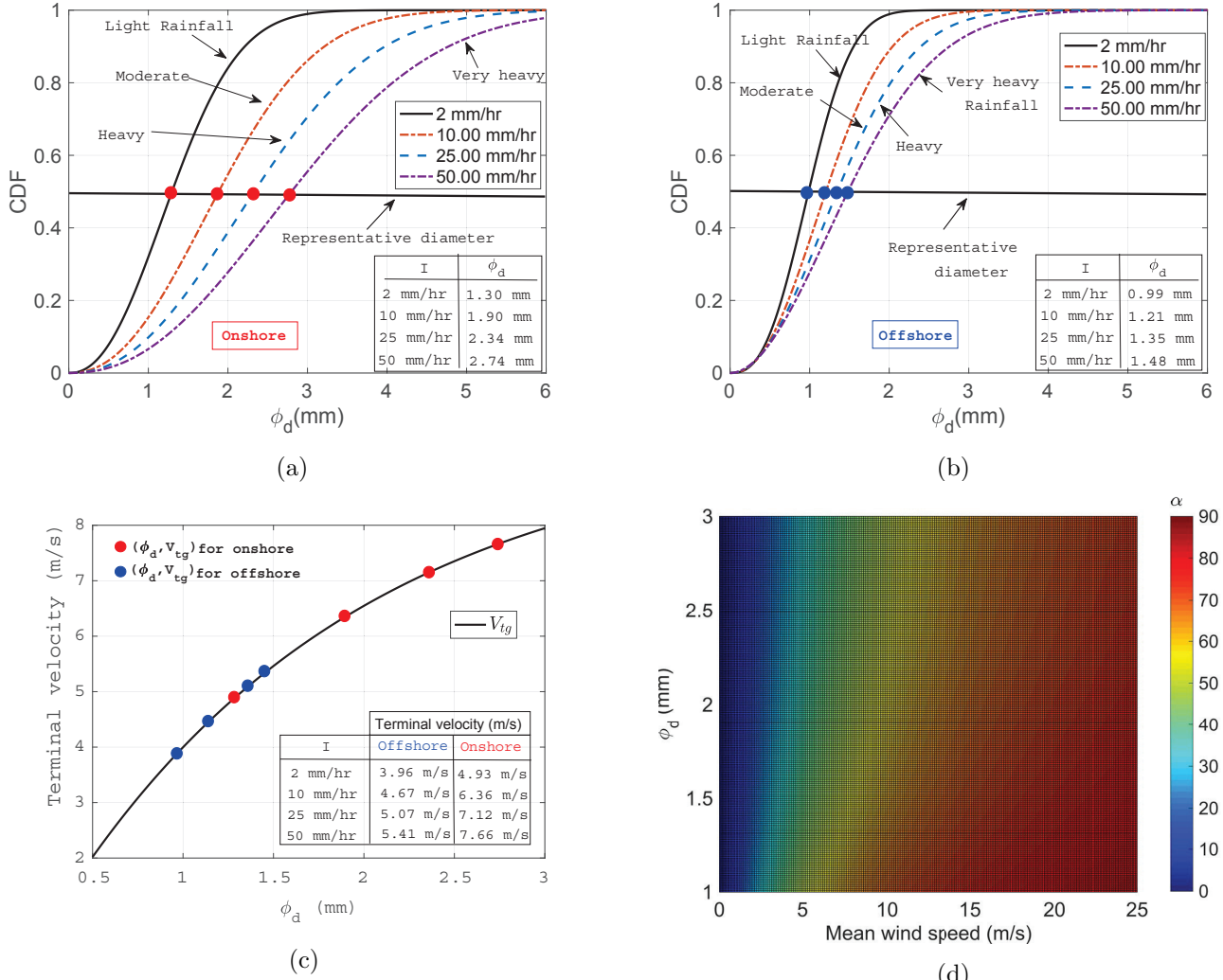


Figure 8: Choice of ϕ_d for different I (a) Onshore - Best distribution (b) Offshore - distribution by [25] (c) V_{tg} (red - onshore; blue-offshore) (d) Variation of α (degrees) with varying ϕ_d and U_w

196 20 random seeds were analysed to consider the statistical uncertainty. The random seeds were considered
 197 in this study for the generation of turbulence boxes as well as for generating irregular waves using the
 198 JONSWAP spectrum [35] with different seed numbers. Each analysis ran for 4000 s, where the first 400
 199 s were filtered out to avoid start-up effects.

200 Rainfall conditions:

201 As already mentioned before, Best's distribution [27] is used to represent the rainfall scenario under
 202 both onshore and offshore conditions, and a suitable droplet size is selected for different values of I .
 203 Nevertheless, a standalone comparative study is presented separately to determine the effect of DSDs on
 204 the leading edge erosion of WTBs and how site-specific rainfall conditions can affect the overall LEE. Four
 205 different rainfall intensities (I) are considered for both onshore and offshore conditions: (1) light rainfall

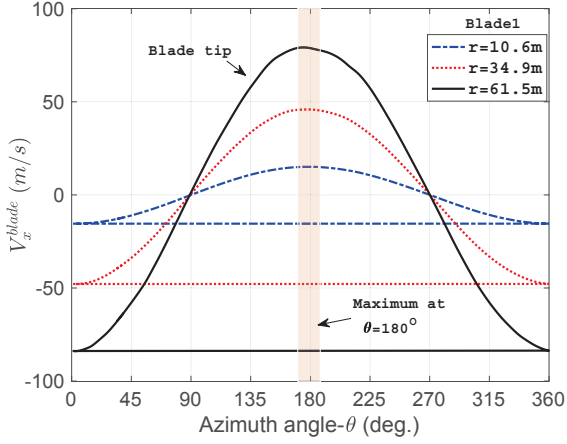
206 (2 mm/hr), (b) moderate rainfall (10 mm/hr), (c) heavy rainfall (25 mm/hr), and (d) very heavy rainfall
 207 (50 mm/hr). Based on these values of I , the rain droplet size (ϕ_d) is determined from the DSDs given by
 208 Eq. (5) and Eq. (6) for onshore and offshore conditions, respectively, and are shown in Figures 8(a)-(b).
 209 The points where the black horizontal line intersects the cumulative distribution function (CDF) curve
 210 correspond to the representative ϕ_d considered in the study, i.e., $\phi_d = 1.30, 1.90, 2.34, 2.74$ mm for
 211 different values of I representing onshore conditions and $\phi_d = 0.99, 1.21, 1.35, 1.48$ mm for different
 212 values of I representing offshore conditions. It can be seen from these figures that Best's distribution
 213 for onshore conditions generally predicts larger droplet size for a given rainfall intensity compared to
 214 offshore DSDs, and the differences in their estimates are significant for a higher rainfall intensity. For
 215 instance, the percentage difference between the predicted ϕ_d for the onshore and offshore rainfall scenarios
 216 is approximately 27% and 60% for $I = 2\text{mm/hr}$ and $I = 50\text{mm/hr}$, respectively. Furthermore, V_{tg} are
 217 obtained for different ϕ_d based on Eq. (4) for both onshore and offshore conditions and are represented
 218 by red and blue dots, respectively (Figure 8(c)). Finally, using Eq. (3), the droplet impact angles (α) are
 219 obtained for different combinations of U_w , V_{tg} and ϕ_d and are presented in Figure 8(d).

220 RESULTS AND DISCUSSION

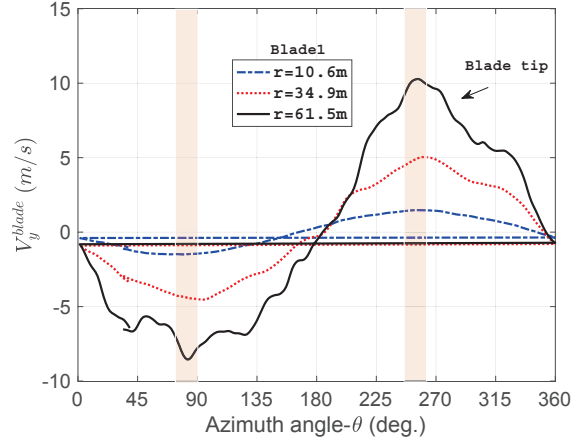
221 In this section, the results for the velocities of the rotating blade are presented first and are discussed
 222 at different azimuth angles and radial positions. Furthermore, the effects of the (a) rainfall intensity, (b)
 223 wave-induced loads, and (c) turbulence intensity on the impact velocities and erosion damage rates are
 224 discussed. Note that for all the cases, 'Blade 1' of the WT is used for discussion.

225 I. Blade speed at different azimuth angles (θ) and radial positions (r)

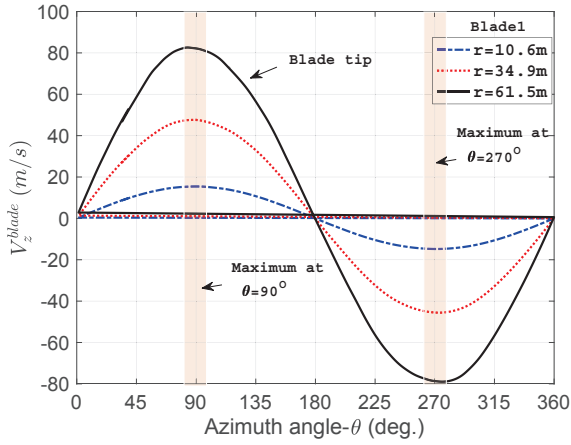
226 Figures 9(a)-(c) present the blade velocity in the global x, y and z -directions, respectively, for the case
 227 of $U_w = 20\text{m/s}$, $TI = 0.06$, corresponding to an onshore wind turbine. The results are presented at
 228 different blade azimuth angles (θ) and three different positions along the blade length. The velocity of
 229 the rotating blade is highest in the rotor plane (xz), with the blade velocity being the largest in the x and
 230 z directions. However, the velocity of the blade in the global y -direction (V_y^{blade}) is smaller, and its peak
 231 value is close to 11 m/s compared to V_x and V_z , where the peak velocity can be in the range of 80 m/s.
 232 Additionally, as expected, the blade tip shows the largest velocity for all cases and thus will be used for
 233 discussion of the results in subsequent sections. Furthermore, the velocity of the blade in the x -direction



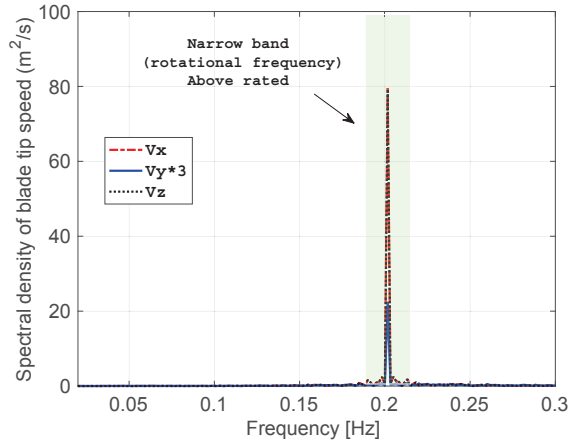
(a)



(b)



(c)



(d)

Figure 9: Comparison of (a) V_x^{blade} (b) V_y^{blade} (c) V_z^{blade} at different θ and $r = 10.4, 34.9, 61.5m$ (d) Spectral density of blade tip speed ($U_w = 20m/s$)

234 has a positive peak value at $\theta = 180^\circ$ and a negative peak value at $\theta = 0^\circ$. On the other hand, V_z^{blade}
 235 has the highest positive impact velocity at $\theta = 90^\circ$ and the corresponding negative velocity at $\theta = 270^\circ$.
 236 This negative velocity at $\theta = 270^\circ$ is expected to give the largest relative impact velocity between rain
 237 and the rotating blade (\vec{V}_{imp}) due to the direction of rainfall in the opposite direction. It is also evident
 238 from the figure that V_z^{blade} shows a perfect smooth sinusoidal curve. However, V_y^{blade} is affected by TI ,
 239 and thus, a perfect sinusoidal smooth function is not obtained, the effect of which is critical at the blade
 240 tip. Nevertheless, the spectral density curve of the blade tip speed shown in Figure 9(d) clearly shows
 241 narrow band behaviour and represents the dominating frequency defined by the power curve of WT.

242 II. Effects of the rainfall intensity (I)

243 Figure 10(a) presents the comparison between the relative impact velocity for the rotating blade tip ($r =$
244 $61.5m$) and a single rain droplet corresponding to different $I = 2mm/hr, 10mm/hr, 25mm/hr, 50mm/hr$.
245 The results are presented at different values of $\theta \in [0^\circ, 360^\circ]$ and for a case of an onshore wind turbine
246 operating at $U_w = 20m/s$ (i.e., above the rated wind speed) and having steady wind conditions ($TI = 0$).
247 Note that for all the cases of rainfall intensities and corresponding U_w , the droplet impact angle (α)
248 varies (see Figure 8(d)) and is considered in all the results presented hereafter. It can be seen from
249 the figure that the impact velocity between the blade and the rain droplet varies cyclically, where it is
250 least at approximately $\theta = 90^\circ$, and highest around $\theta = 270^\circ$ - a percentage difference of approximately
251 13% is found between the maximum and minimum values for rainfall conditions representing the largest
252 rainfall intensity ($I = 50 mm/hr$). This implies that rain-induced fatigue damage accumulation and
253 the subsequent erosion damage rate of a WTB coating would vary with varying blade azimuth angles
254 traversed during the rotation of the blade.

255 Furthermore, it is also found that the relative impact velocity between the blade tip and the rain drops
256 increases with increasing rainfall intensity, given that rain corresponding to large rainfall intensity yields a
257 larger droplet size (as seen from DSDs presented before) and therefore is associated with a higher terminal
258 velocity of the drop. Given that V_y^{blade} and V_z^{blade} are the dominating blade responses that influence
259 \vec{V}_{imp} for varying rainfall characteristics (and including α and V_d , see Eq. (1)), only these parameters
260 will be considered for the assessment of erosive variables in our subsequent discussions. Therefore, for
261 all the discussions hereafter, the velocity of the blade in the x-direction (V_x^{blade}) is filtered out for a
262 lucid scale of comparison among different erosive variables for varying environmental parameters. For
263 instance, Figure 10(b) presents the impact velocity between the rotating blade tip ($r = 61.5m$) and rain
264 droplet corresponding to different values of $I = 2mm/hr, 10mm/hr, 25mm/hr, 50mm/hr$, with the V_x^{blade}
265 component filtered out. The results are presented at different values of $\theta \in [0^\circ, 360^\circ]$ and for a case of
266 an onshore wind turbine operating at $U_w = 20m/s$ (i.e., above the rated wind speed) and having steady
267 wind conditions ($TI = 0$). It can be seen from the figure that the impact velocity between the blade and
268 the rain droplet varies cyclically, where it is least at approximately $\theta = 90^\circ$ and highest at approximately
269 $\theta = 270^\circ$. This trend is expected based on the results presented before in Figure 9(a)-(c), where V_y^{blade}
270 and V_z^{blade} reached their negative peak values at $\theta = 270^\circ$ and thus contributed the most to the relative
271 impact velocity. A magnified view is also presented in Figure 10(c), showing the differences in the impact
272 velocity for different rainfall intensities, which are found in the range of 2-5%. From the figure, there

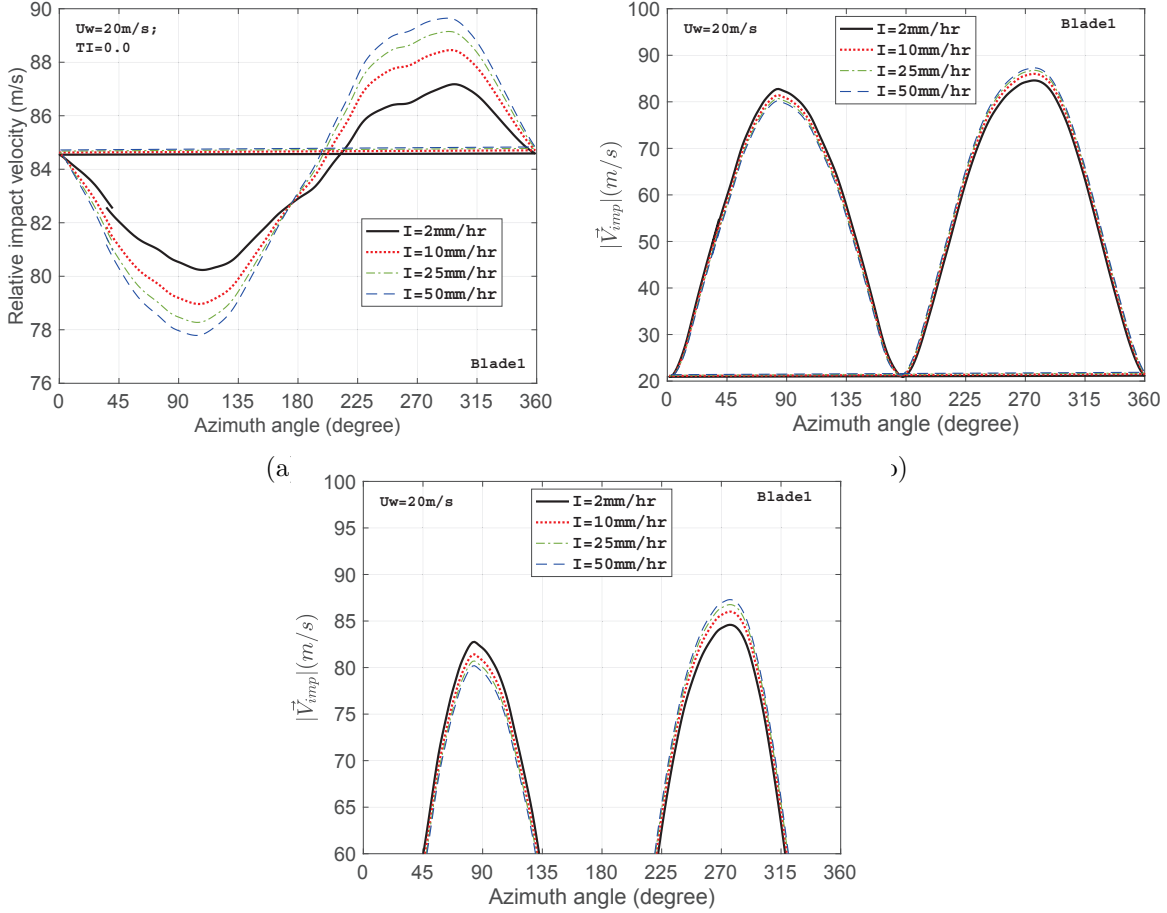


Figure 10: Comparison of (a) $|\vec{V}_{imp}|$ for $I = 2mm/hr$, $10mm/hr$, $25mm/hr$, $50mm/hr$ (b) magnified view; comparison of (c) \dot{D}_i

273 might be thoughts that there are not many differences in the impact velocities of the blade tip for different
 274 rainfall intensities and that only the blade tip speed dominates erosion while operating at a given wind
 275 speed. This is also represented in Figure 11(a), where the rain droplet-induced water hammer pressure
 276 (p_{wh}) developed onto the blade at different blade azimuth angles (considering the material properties
 277 of the PET coating listed in Table 1) and for different $I = 2mm/hr, 10mm/hr, 25mm/hr, 50mm/hr$ is
 278 presented. The difference in p_{wh} is minor and is found in the range of 2-5% for different I , given that p_{wh}
 279 depends linearly on \vec{V}_{imp} .

280 However, it should be noted that the most important erosive parameters, i.e. the erosion damage
 281 rate (\dot{D}_i) is proportional to \vec{V}_{imp} with a power of 6.7 (see Eq. (8)). In addition, the erosion damage rate
 282 (\dot{D}_i) is directly proportional to q , i.e., the number of droplets in a cubic volume of rain, and increases
 283 with increasing I . Therefore, even a modest increase in the impact velocity due to increasing rainfall
 284 intensity is expected to substantially increase the \dot{D}_i . This can be seen from Figure 11(b), where the

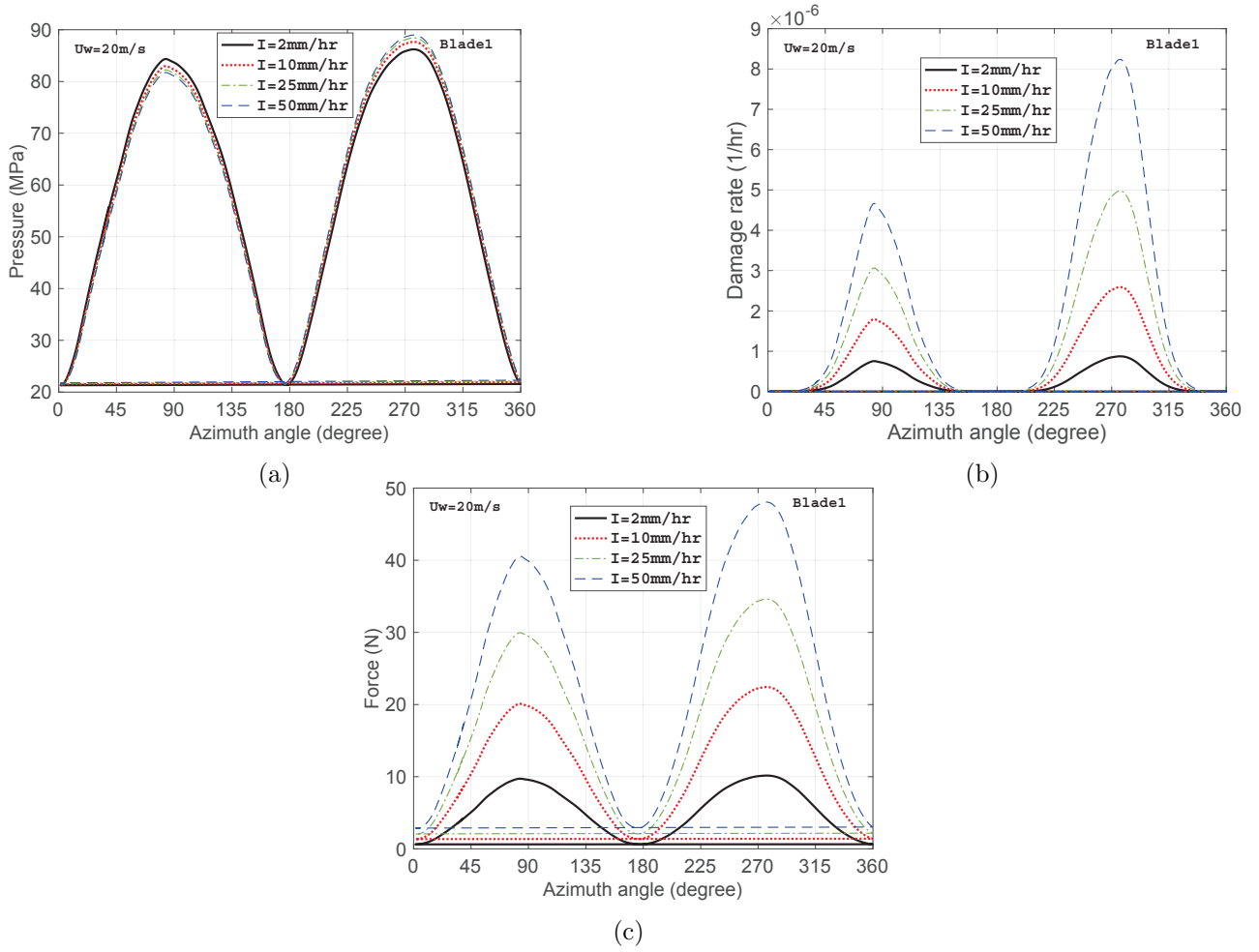


Figure 11: Comparison of (a) p_{wh} (b) \dot{D}_i (c) F_{imp} for $I = 2 \text{ mm/hr}$, 10 mm/hr , 25 mm/hr , 50 mm/hr

285 erosion damage rate is compared for the blade tip at different rainfall intensities, different θ and $U_w =$
286 20 m/s . The results clearly show that there is a substantial increase in the \dot{D}_i , which is more than 85%
287 when exposed to very heavy rainfall compared to blades exposed to light rainfall. These results clearly
288 demonstrate that for a given blade tip speed, different magnitudes of rainfall intensity are expected to have
289 varying rain erosion performance. Thus, these aspects need to be considered when developing a control
290 algorithm for reducing the tip speed of the blade. In this way, the incubation period ($1/\dot{D}_i$) of the blade
291 can be extended. Figure 11(c) further presents the comparison between the peak impact forces caused
292 between the rotating blade tip ($r = 61.5 \text{ m}$) and rain droplet corresponding to different rainfall intensities
293 ($I = 2 \text{ mm/hr}$ 10 mm/hr 25 mm/hr 50 mm/hr). Given that the peak force is proportional to \vec{V}_{imp} and ϕ_d
294 with a power of 2 (see Eq. (7)), a noticeable difference can be seen in the peak forces developed by heavy
295 rainfall compared to light rainfall at different θ . Overall, rainfall intensity is an essential parameter to
296 included in LEE analysis.

297 III. Effects of wave-induced loads (H_s, T_p) on tower top responses

298 In this section, the effects of wave-induced loads on the LEE of WTBs in terms of $|\vec{V}_{imp}|$ and the erosion
 299 damage rate (\dot{D}_i) are discussed. Since collinear wind-wave conditions are considered in the study, only
 300 the motion of the monopile in the fore-aft direction will affect the results for $|\vec{V}_{imp}|$ and are discussed
 hereafter.

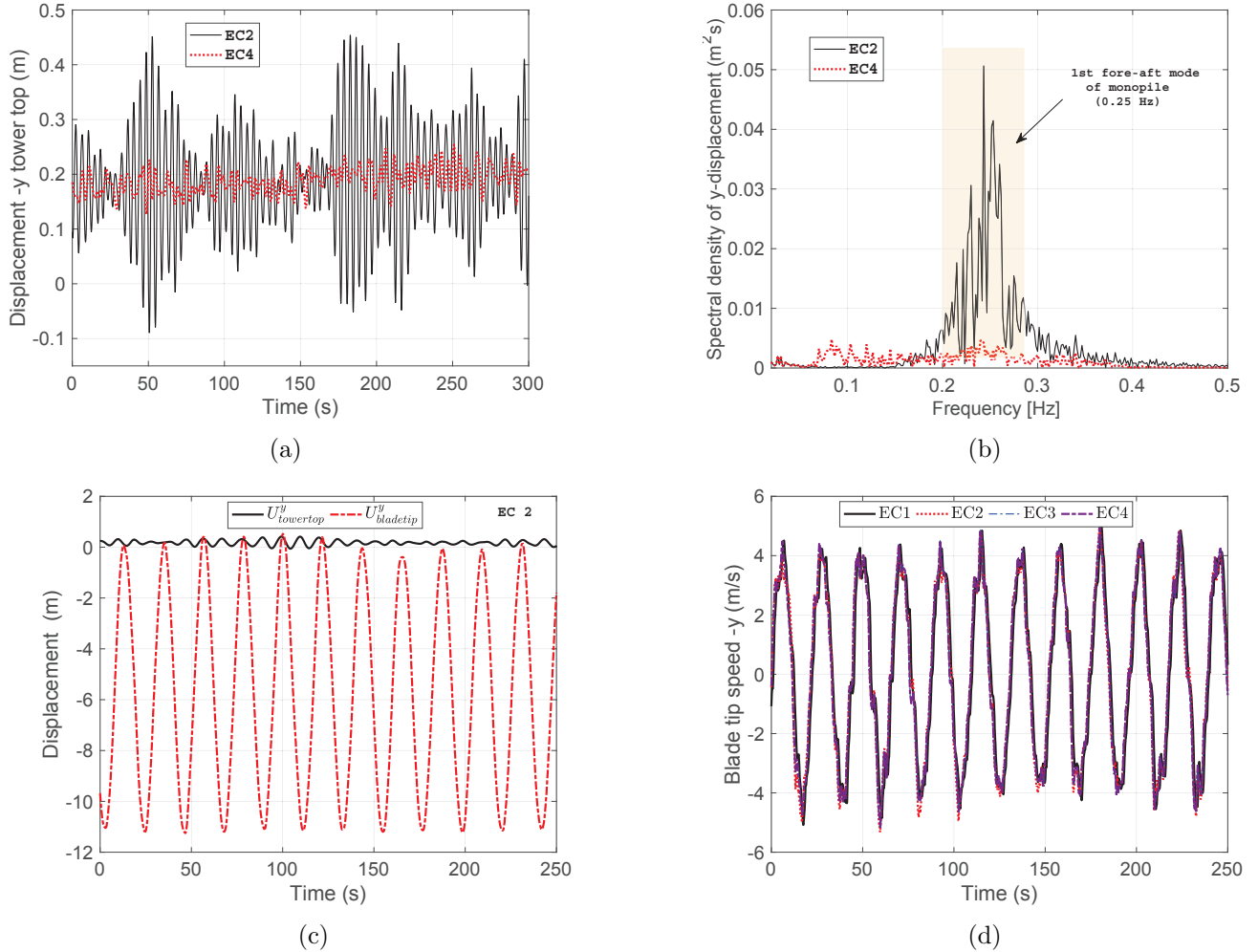


Figure 12: Comparison of (a) U_{hub}^y and its (b) Spectral density for EC2 and EC4; Comparison of (c) U_{hub}^y and U_{blade}^y (d) V_y^{blade}

301

302 Figure 12(a) compares the motion of the tower top in the fore-aft direction (y -global) for a load case
 303 corresponding to $H_s = 2.30m$, $T_p = 4.2s$ (EC2) and $H_s = 2m$, $T_p = 12s$ (EC4) together with a constant
 304 $U_w = 6m/s$, $TI = 0.06$ (below rated). It can be seen that the tower top has large responses in the fore-aft
 305 direction compared to $T_p = 12s$ and this is due to the fact that $T_p = 4.2s$ matches with the eigenfrequency
 306 of the turbine, thereby causing resonance. A spectral density curve for the tower top motion is compared
 307 for EC2 and EC4 in Figure 12(b), where a high peak is seen at the resonance frequency for load case EC2.

308 Nevertheless, the motion is still minor compared to the motion of the blade itself in the y -direction. This
 309 is due to the presence of aerodynamic damping from the rotating blades, which reduces the amplification
 310 of responses at resonance. For instance, Figure 12(c) compares the motion of the tower top and blade in
 311 the global y -direction, and it is evident that the contribution of the monopile is minor. This implies that
 312 the wave-induced tower top motion is not expected to significantly change V_y^{blade} . This can be confirmed
 313 from Figure 12(d), where V_y^{blade} is compared for EC1, EC2, EC3 and EC4, where EC1 corresponds to the
 314 case of an onshore wind turbine. The contribution of wave-induced loads is negligible, as the results for
 315 all the load cases completely overlap with each other except EC2, which exhibits a minor difference due
 316 to the resonance effects discussed above.

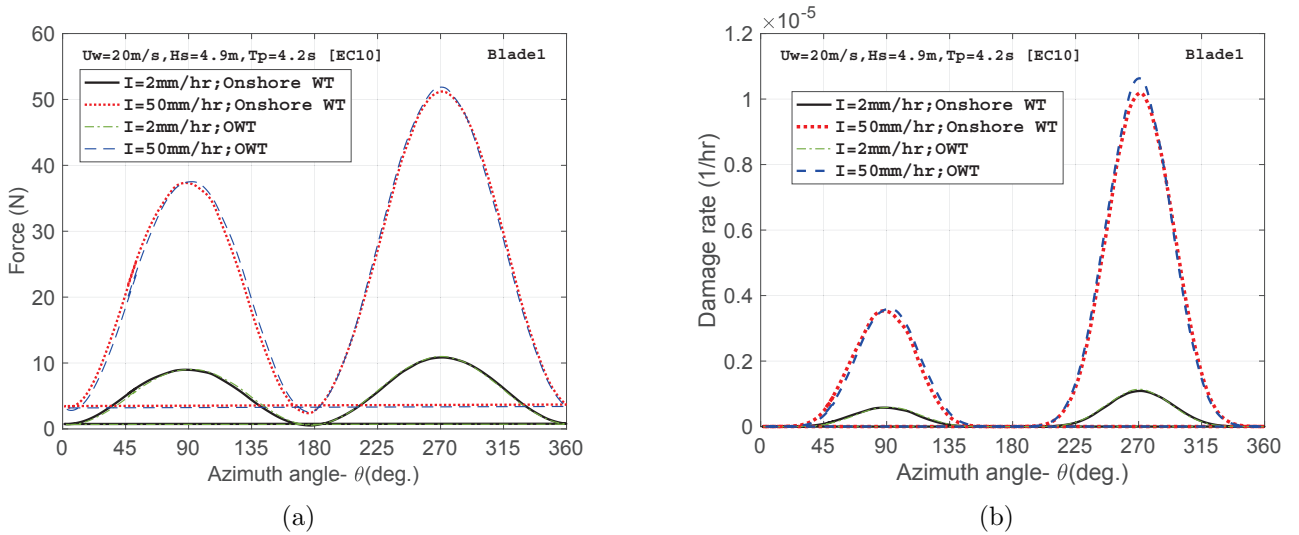


Figure 13: Comparison of (a) F_{imp} (b) \dot{D}_i , between onshore and offshore wind turbine for EC10 ($H_s = 4.9m, T_p = 4.2s, U_w = 20m/s$) and $I = 2mm/hr, 50mm/hr$

317 Subsequently, the impact forces and erosion damage rates are compared (Figures 13(a)-(b)) between
 318 the onshore and offshore wind turbines for EC10. This case is the most critical for offshore wind turbines
 319 due to large wave heights ($H_s = 4.9m$) and $T_p = 4.2s$, which match the resonance frequency. These results
 320 are presented for two different rainfall intensities ($I = 2mm/hr; 50mm/hr$), the above rated wind speed
 321 ($U_w = 20m/s$) and $TI = 0.12$. The results show that the differences in the impact forces and erosion
 322 damage rate are minor for onshore and offshore wind turbines under very heavy rainfall conditions and
 323 negligible for light, moderate and heavy rainfall conditions. Overall, it can be implied from the results
 324 that LEE is not affected by wave-induced tower top responses; therefore, this parameter is not essential
 325 for LEE modelling. Note that the present paper only considers a monopile-based fixed offshore wind
 326 turbine. These results will be compared in the future for floating offshore wind turbines.

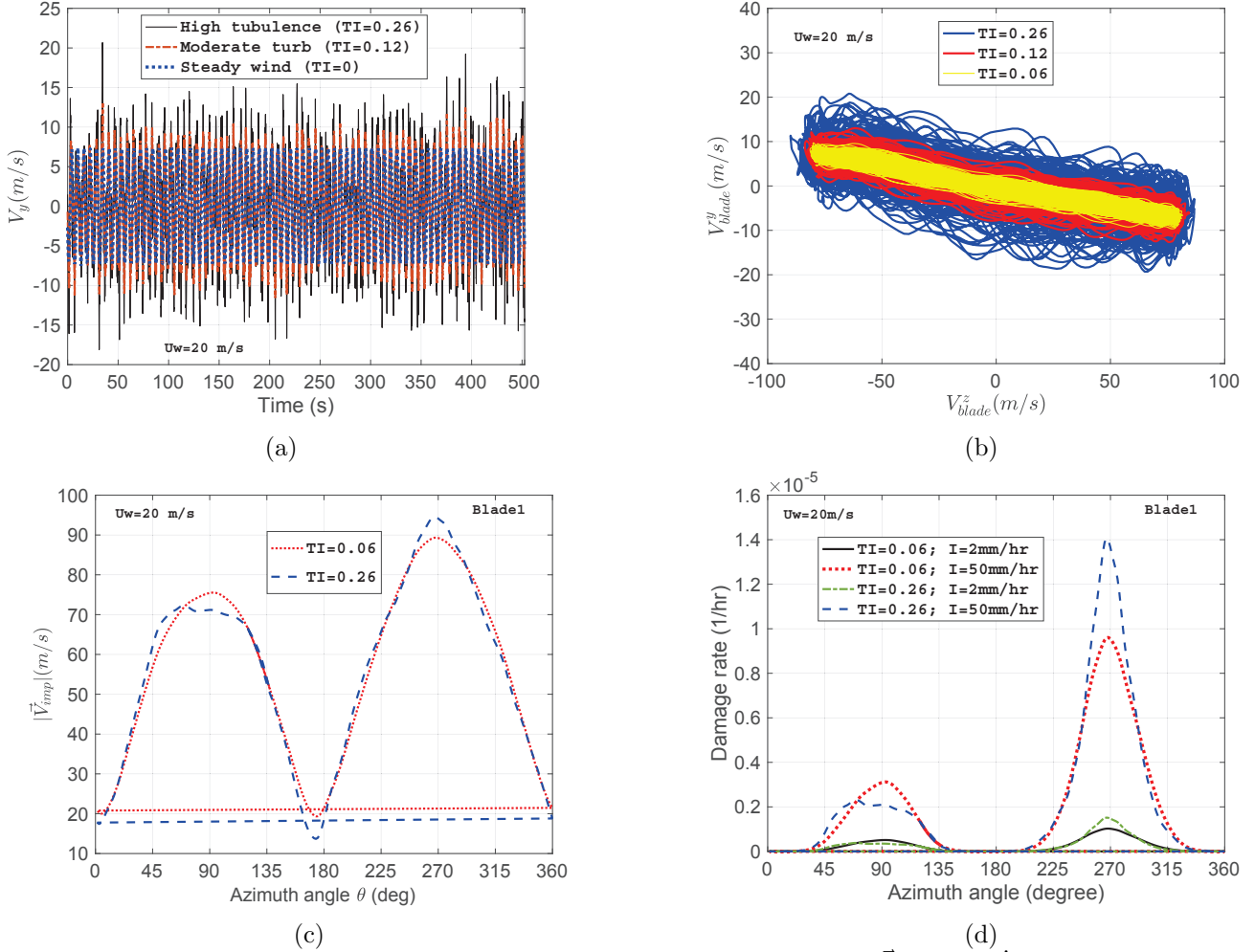


Figure 14: Comparison of (a) V_y^{blade} (b) blade tip speed in yz -plane (c) $|\vec{V}_{imp}|$ (d) \dot{D}_i for $TI = 0.06, 0.26$ $I = 2mm/hr$ $50mm/hr$ and $U_w = 20m/s$

327 IV. Effects of turbulence intensity (TI)

328 In this section, the effects of TI on the LEE are discussed. Figure 14(a) compares the velocity of the
 329 rotating blade in the global y -direction for three values of $TI = 0.0, 0.12, 0.26$ and $U_w = 20m/s$. It
 330 is evident from the figure that considering only the steady wind for the LEE analysis, underpredicts
 331 V_y^{blade} . Furthermore, peak values for V_y^{blade} increase from 7 m/s for $TI = 0.0$ to more than 20 m/s for
 332 $TI = 0.26$, thereby demonstrating the significance of TI for LEE modelling. Similar observations can
 333 be seen in Figure 14(b), where the velocity of the lifted blade in the critical yz -plane is compared for
 334 values of $TI = 0.06, 0.12, 0.26$ and $U_w = 20m/s$. It can be seen from the figure that V_y^{blade} increases
 335 with increasing TI , and there are minor influences on V_z^{blade} . Furthermore, Figure 14(c) compares the
 336 $|\vec{V}_{imp}|$ for two $TI = 0.06, 0.26$ and at θ . The difference in $|\vec{V}_{imp}|$ for both cases is minor; however,
 337 there is a substantial influence on the erosion damage rate of LE. Figure 14(d) compares the values of

338 \dot{D}_i for ($TI = 0.06, 0.26$) and two rainfall intensities ($I = 2mm/hr, 50mm/hr$). The turbulence intensity
339 is found to have a significant influence on the erosion damage rate, and the effect is most critical for
340 very heavy rainfall conditions ($I = 50mm/hr$) and high turbulent wind associated with gust conditions
341 ($TI = 0.26$). Overall, TI is an important parameter to included for LEE modelling. The results also show
342 that the current state-of-the-art method, where the steady power curve of the wind turbine is included
343 for the LEE analysis, would underpredict the results.

344 **V. Effects of the droplet size distributions (DSDs) used for representing rainfall** 345 **scenarios at onshore and offshore locations**

346 In our previous discussions, Best's DSD [27] was used to analyse LEE for representing rainfall scenarios
347 at both onshore and offshore locations. This is because the distribution has been applied extensively
348 in the literature for LEE. Nevertheless, a standalone comparative study is presented here to check the
349 effect of the DSDs on the LEE of WTBs and to assess how site-specific rainfall conditions can affect the
350 overall erosion damage rate. As discussed in section 3, the rainfall scenario onshore is given by Best's
351 DSD [27], whereas the rainfall scenario offshore is given by the DSD developed in [25]. In the onshore and
352 offshore rain described through the above DSDs, the main distinction is the difference in the estimations
353 of representative droplet sizes for a given rainfall condition. Thus, there will be distinct droplet sizes given
354 the same rainfall intensity for onshore and offshore locations. For instance, an onshore rainfall representing
355 light rainfall conditions ($I = 2mm/hr$) using Best's DSD represents rain comprising a median droplet size
356 of 1.30 mm, whereas the same rainfall condition for offshore rain represents a relatively smaller median
357 droplet size of 0.99 mm. Similarly, the very heavy rainfall condition ($I = 50mm/hr$) described by Best's
358 DSD for onshore rain has a median droplet size of 2.34 mm, whereas for offshore rain $I = 50mm/hr$, and
359 the droplet size is 1.48 mm.

360 Figure 15(a) compares the impact velocity between the rotating blade tip ($r = 61.5m$) and a single rain
361 droplet for onshore and offshore scenarios with two different values of I ($I = 2mm/hr$ and $I = 50mm/hr$).
362 Each of these curves represents varying median droplet sizes and different intensities of rain at onshore and
363 offshore rainfall - median droplet sizes of 1.30 mm (light rainfall onshore), 0.99 mm (light rainfall offshore),
364 2.34 mm (very heavy rainfall onshore) and 1.48 mm (very heavy rainfall offshore). Furthermore, the results
365 are presented for different $\theta \in [0^\circ, 360^\circ]$ and for a case of a wind turbine operating at $U_w = 20m/s$ (i.e.,
366 above the rated wind speed) and having steady wind conditions ($TI = 0$). No wave-induced loads (H_s, T_p)
367 are considered acting on the offshore wind turbine to ensure a standalone comparison of the erosion damage

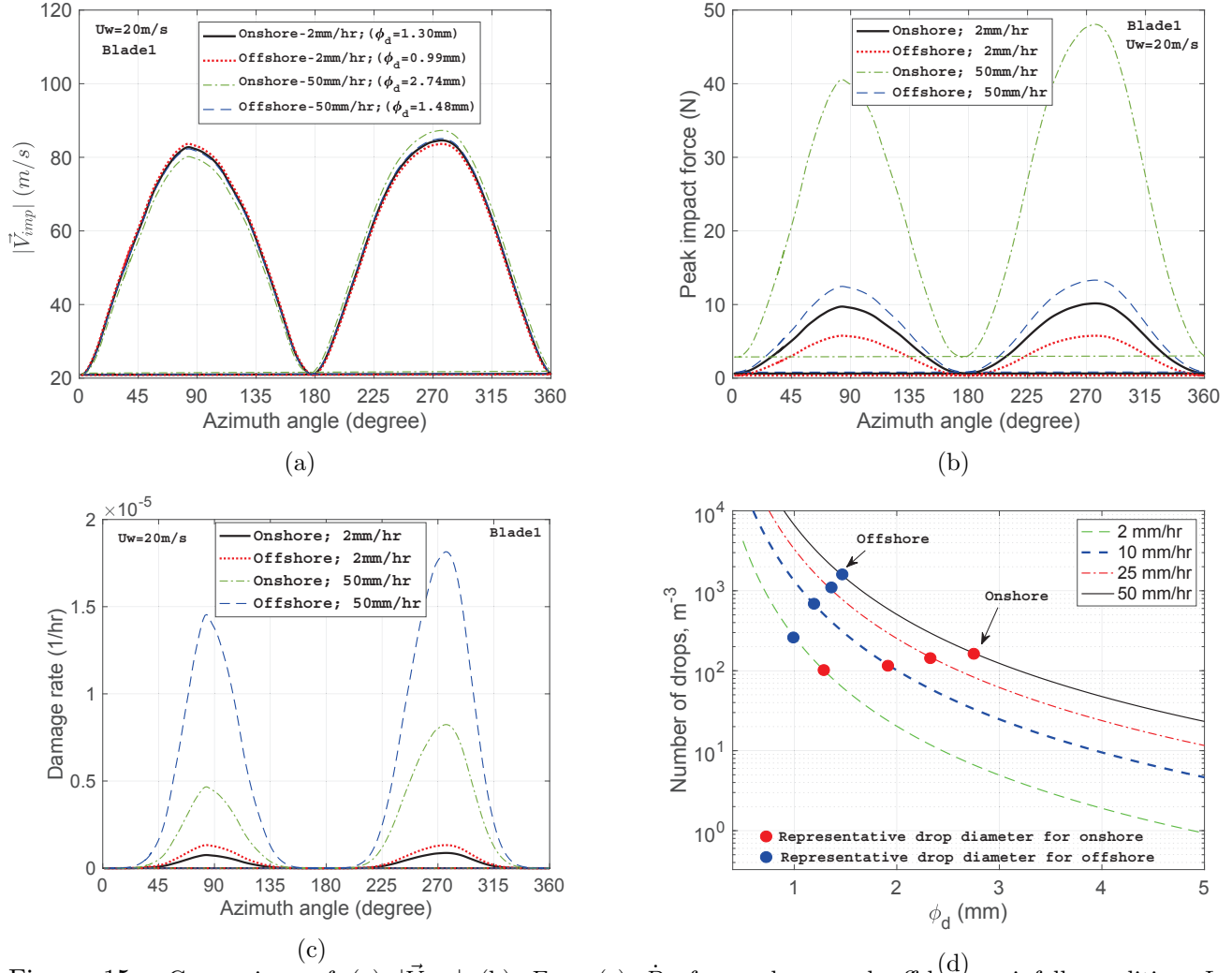


Figure 15: Comparison of (a) $|\vec{V}_{imp}|$ (b) F_{imp} (c) \dot{D}_i for onshore and offshore rainfall condition $I = 2 \text{ mm/hr}$, 50 mm/hr (d) q for several ϕ_d and $I = 2 \text{ mm/hr}$, 10 mm/hr , 25 mm/hr , 50 mm/hr

368 rates due to varying DSDs. The figure shows that the values of the impact velocities for blade exposure to
 369 onshore and offshore rainfall scenarios differ slightly from each other for a given I . The impact velocities
 370 are found to be higher for the onshore scenario - the highest percentage difference between the $|\vec{V}_{imp}|$
 371 for the onshore and offshore rainfall scenarios is in the range of 2-5% for very heavy rainfall conditions
 372 ($I = 50 \text{ mm/hr}$). This is because Best's distribution estimates a larger ϕ_d for a given rainfall intensity
 373 (I) and is associated with a higher terminal velocity of the droplet compared to the offshore DSD. These
 374 results are also reflected when comparing the peak impact forces (figure 15(b)) between the rotating blade
 375 tip ($r = 61.5 \text{ m}$) and a single rain droplet (for onshore and offshore rainfall scenarios) for two different
 376 values of I ($I = 2 \text{ mm/hr}$ and $I = 50 \text{ mm/hr}$). Given that the peak impact force is proportional to \vec{V}_{imp}
 377 and ϕ_d with a power of 2 (see Eq. (7)), a noticeable difference can be seen in the peak forces between the
 378 droplet and blade impact for onshore and offshore rainfall scenarios, with the largest value found for the

379 case of an onshore DSD and for the highest I .

380 However, a very interesting result can be seen when comparing the erosion damage rates (\dot{D}_i) for
381 a WTB exposed to onshore and offshore rainfall scenarios. Here, the erosion damage rate is calculated
382 by considering the contribution from multiple rain droplets that are contained in a given rain scenario.
383 The number of droplets in a given rain scenario is calculated according to Eq. (9), where it is assumed
384 that the entire rainfall volume for a given intensity consists of rain droplets with diameters equal to the
385 median droplet size. It can be seen from Figure 15(c) that unlike the impact velocity and peak impact
386 forces mentioned above, the erosion damage rate contributed from multiple rain droplets is found to
387 be significantly large when exposed to the offshore rainfall scenario. The highest percentage difference
388 between the \dot{D}_i for onshore and offshore rainfall scenarios is found in the range of 100-110% for $I =$
389 50 mm/hr . This is because \dot{D}_i is directly proportional to q (Eq. (8)), i.e., number of water droplets
390 in a unit cubic volume of rain, which is significantly higher for the offshore rainfall scenario than that
391 onshore. Again, this is attributed to the fact discussed earlier that the offshore DSD predicts a much
392 smaller droplet size (ϕ_d) for a given I compared to Best's DSD, thereby yielding more drops in a unit
393 volume of rain. Note that q in Eq. (9) is inversely proportional to the cubic power of ϕ_d and consists
394 of V_{tg} in the denominator with the ϕ_d term in an exponential function. Overall, even a modest change
395 in the droplet size significantly influences q and \dot{D}_i . For instance, figure 15(d) compares q for different
396 combinations of rainfall intensities and ϕ_d . The number of drops in a given rain scenario using the offshore
397 DSD for a given I is notably larger than the onshore DSD (please note the y-axis, which is plotted on
398 a logarithmic scale). This implies that during the blade rotation, low impact forces and pressures are
399 developed due to single rain droplet impact for offshore conditions since offshore rain determined using
400 the DSD from [25] consists of a smaller ϕ_d for a given I . However, there would be several such impacts
401 (as q is significantly larger) for a rainfall scenario described through offshore DSD compared to Best's
402 DSD. This would cause a larger fatigue damage accumulation and erosion damage rate of a WTB due
403 to exposure to rain. Overall, the rainfall scenario for offshore conditions, described based on the DSD
404 by [25], is found to have a significant effect on the erosion damage rate of a WTB and is an essential
405 parameter for modelling.

406 CONCLUSIONS

407 The present paper performs aero-hydro-servo-elastic simulations on the rotating blade and investigates
408 whether there are differences in erosion of blades due to (1) varying rainfall conditions modelled using
409 different droplet size distributions for onshore and offshore locations, in combination with (2) winds of
410 varying turbulence intensities and (3) wave-induced loads. The main aim of the study was to provide
411 guidelines on whether all these environmental parameters must be included in LEE modelling. Different
412 precipitation parameters for both onshore and offshore locations are considered through an in-house code,
413 and erosion variables that include impact velocities, erosion damage rates, peak impact forces and impact
414 pressures are compared at different blade azimuth angles. An analytical surface fatigue damage model
415 based on Springer’s model [8] is considered together with fatigue properties for a PET-based thermoplastic
416 leading edge coating. The following points are the main conclusions that are found through the analysis
417 performed in the study regarding guidelines for environmental parameters to include for LEE modelling:

418 • The rainfall intensity (I) is an essential parameter for analysing LEE of a WTB. The results from
419 the study show that although there is a minor change in the impact velocity and impact pressure between
420 individual rain droplets and rotating blades at different values of I and blade azimuth angles, a substantial
421 increase is found in the erosion damage rate (\dot{D}_i) of a WTB. The % difference in \dot{D}_i of a WTB is more
422 than 85% when exposed to very heavy rainfall compared to blades exposed to light rainfall. Overall,
423 for a given blade tip speed and operating wind condition, different magnitudes of rainfall intensities are
424 expected to have varying rain erosion performances.

425 • The turbulence intensity (TI) is also found to be an important parameter to include for LEE
426 modelling and has rarely been considered in the literature. Again, the results show that the turbulence
427 intensity minorly influences the impact velocity due to a single rain droplet impact; however, it has a
428 substantial effect on the overall erosion damage rate due to multiple rain drops. For instance, for the
429 investigated load cases, an 8% increase in the impact velocity is observed when the turbulence intensity
430 increases from 6% to 26%, which demonstrates an increase in the erosion damage rate by more than 40%.

431 • An investigation is performed to check the effect of DSDs on the LEE of WTBs and to assess how
432 site-specific rainfall conditions, described through different DSDs, can affect the overall erosion damage
433 rate. The rainfall scenario onshore is given by Best’s distribution [27], whereas the rainfall scenario
434 offshore is given by the DSD developed in [25]. It was found that the erosion damage rate for a WTB
435 is significantly larger when exposed to the offshore rainfall scenario compared to the onshore scenario -

436 the highest percentage difference between the values of \dot{D}_i for onshore and offshore rainfall scenarios is
437 in the range of 100-110% for very heavy rainfall conditions ($I = 50mm/hr$). This is found because \dot{D}_i is
438 directly proportional to the number of water droplets in a unit cubic volume of rain and is significantly
439 higher for the offshore rainfall scenario than that onshore. Overall, DSDs are an important factor for
440 LEE modeling.

441 • Finally, wave induced loading is found to be an unimportant parameter to include for LEE modelling,
442 and no substantial influence is found on LEE of a WTB. However, this conclusion is limited to a relatively
443 stiff bottom fixed monopile-type offshore wind turbine. In the future, similar investigations will be
444 performed on floating offshore wind turbines.

445 **LIMITATIONS AND FUTURE WORK**

446 The investigations performed in this paper are limited to short-term analyses. Accurate evaluation of
447 long-term LEE requires site-specific environmental data, information on the wind turbine operational
448 condition, and a probabilistic framework. These aspects will be considered in future work. Additionally,
449 Springer's model [8] used in this study for estimating the erosion damage rate for the coating material
450 needs to be validated and further improved by considering factors such as rest periods and viscoelastic
451 properties of the elastomeric coatings. Furthermore, given that the atmospheric stability conditions vary
452 for onshore and offshore conditions, their effects on the erosion damage rate will be investigated in further
453 studies. Additionally, all these investigations and results will be compared in the future for floating-based
454 offshore wind turbines.

455 **ACKNOWLEDGMENT**

456 This work was funded through the WINDCORE project having subsidy scheme TSE-18-04-01-Renewable
457 energy project with project number TEHE1180113. The authors also appreciate anonymous reviewers of
458 Journal of Offshore Mechanics and Arctic Engineering (JOMAE) and ASME 39th International Conference
459 on Ocean, Offshore and Arctic Engineering (OMAE 2020) for their thoughtful comments and suggestions.
460 Weifei Hu gratefully acknowledges the funding from the National Natural Science Foundation of China
461 (Grant No. 51905475).

References

- [1] Verma, A. S., Vedvik, N. P., and Gao, Z., 2019. “A comprehensive numerical investigation of the impact behaviour of an offshore wind turbine blade due to impact loads during installation”. *Ocean Engineering*, **172**, pp. 127–145.
- [2] Verma, A. S., Jiang, Z., Vedvik, N. P., Gao, Z., and Ren, Z., 2019. “Impact assessment of a wind turbine blade root during an offshore mating process”. *Engineering Structures*, **180**, pp. 205–222.
- [3] Verma, A. S., Jiang, Z., Ren, Z., Gao, Z., and Vedvik, N. P., 2019. “Response-based assessment of operational limits for mating blades on monopile-type offshore wind turbines”. *Energies*, **12**(10), p. 1867.
- [4] Verma, A. S., Vedvik, N. P., Haselbach, P. U., Gao, Z., and Jiang, Z., 2019. “Comparison of numerical modelling techniques for impact investigation on a wind turbine blade”. *Composite Structures*, **209**, pp. 856–878.
- [5] Verma, A. S., Zhao, Y., Gao, Z., and Vedvik, N. P., 2019. “Explicit structural response-based methodology for assessment of operational limits for single blade installation for offshore wind turbines”. In Proceedings of the Fourth International Conference in Ocean Engineering (ICOE2018), Springer, pp. 737–750.
- [6] Hofmann, M., and Sperstad, I. B., 2014. “Will 10 mw wind turbines bring down the operation and maintenance cost of offshore wind farms?”. *Energy Procedia*, **53**, pp. 231–238.
- [7] Mishnaevsky Jr, L., 2019. “Repair of wind turbine blades: Review of methods and related computational mechanics problems”. *Renewable energy*.
- [8] Springer, G. S., 1976. “Erosion by liquid impact”.
- [9] Herring, R., Dyer, K., Martin, F., and Ward, C., 2019. “The increasing importance of leading edge erosion and a review of existing protection solutions”. *Renewable and Sustainable Energy Reviews*, **115**, p. 109382.
- [10] Wisler, R., Jenni, K., Seel, J., Baker, E., Hand, M., Lantz, E., and Smith, A., 2016. “Forecasting wind energy costs and cost drivers: The views of the worlds leading experts”.
- [11] Picture taken under permission from Vattenfall group, <https://group.vattenfall.com/what-we-do/our-energy-sources>

- [12] Picture taken under permission from TNO, <https://www.tno.nl>.
- [13] Picture taken under permission from DURALEEDGE Project, <http://www.duraledge.dk>.
- [14] Slot, H., IJzerman, R., le Feber, M., Nord-Varhaug, K., and van der Heide, E., 2018. “Rain erosion resistance of injection moulded and compression moulded polybutylene terephthalate pbt”. *Wear*, **414**, pp. 234–242.
- [15] Keegan, M. H., Nash, D., and Stack, M., 2014. “Wind turbine blade leading edge erosion: An investigation of rain droplet and hailstone impact induced damage mechanisms”. PhD thesis, University of Strathclyde.
- [16] Eisenberg, D., Laustsen, S., and Stege, J., 2018. “Wind turbine blade coating leading edge rain erosion model: Development and validation”. *Wind Energy*, **21**(10), pp. 942–951.
- [17] Bech, J. I., Hasager, C. B., and Bak, C., 2018. “Extending the life of wind turbine blade leading edges by reducing the tip speed during extreme precipitation events”. *Wind Energ. Sci. Discuss.*
- [18] Chen, J., Wang, J., and Ni, A., 2019. “A review on rain erosion protection of wind turbine blades”. *Journal of Coatings Technology and Research*, **16**(1), pp. 15–24.
- [19] Amirzadeh, B., Louhghalam, A., Raessi, M., and Tootkaboni, M., 2017. “A computational framework for the analysis of rain-induced erosion in wind turbine blades, part i: Stochastic rain texture model and drop impact simulations”. *Journal of Wind Engineering and Industrial Aerodynamics*, **163**, pp. 33–43.
- [20] Verma, A. S., Castro, S. G., Jiang, Z., and Teuwen, J. J., 2020. “Numerical investigation of rain droplet impact on offshore wind turbine blades under different rainfall conditions: A parametric study”. *Composite Structures*, p. 112096.
- [21] Keegan, M. H., Nash, D., and Stack, M., 2013. “On erosion issues associated with the leading edge of wind turbine blades”. *Journal of Physics D: Applied Physics*, **46**(38), p. 383001.
- [22] Castorrini, A., Corsini, A., Rispoli, F., Venturini, P., Takizawa, K., and Tezduyar, T. E., 2016. “Computational analysis of wind-turbine blade rain erosion”. *Computers & Fluids*, **141**, pp. 175–183.

- [23] Verma, A. S., Castro, S. G., Jiang, Z., Hu, W., and Teuwen, J. J., 2020. “Leading edge erosion of wind turbine blades: Effects of blade surface curvature on rain droplet impingement kinematics”. In *Journal of Physics: Conference Series*, Vol. 1618, IOP Publishing, p. 052003.
- [24] Wang, Y., Deng, Y., Liu, Y., Qu, L., Wen, X., Lan, L., and Wang, J., 2019. “Influence of blade rotation on the lightning stroke characteristic of a wind turbine”. *Wind Energy*.
- [25] Herring, R., Dyer, K., Howkins, P., and Ward, C., 2020. “Characterisation of the offshore precipitation environment to help combat leading edge erosion of wind turbine blades”. *Wind Energy Science Discussions*, **2020**, pp. 1–16.
- [26] De Lima, J., 1989. “The influence of the angle of incidence of the rainfall on the overland flow process”. *IAHS Publication (United Kingdom)*.
- [27] Best, A., 1950. “The size distribution of raindrops”. *Quarterly Journal of the Royal Meteorological Society*, **76**(327), pp. 16–36.
- [28] Larsen, T. J., and Hansen, A. M., 2007. “How 2 HAWC2, the user’s manual”.
- [29] Jonkman, J., Butterfield, S., Musial, W., and Scott, G., 2009. “Definition of a 5-mw reference wind turbine for offshore system development”. *National Renewable Energy Laboratory, Golden, CO, Technical Report No. NREL/TP-500-38060*.
- [30] Zhang, R., Zhang, B., Lv, Q., Li, J., and Guo, P., 2019. “Effects of droplet shape on impact force of low-speed droplets colliding with solid surface”. *Experiments in Fluids*, **60**(4), p. 64.
- [31] Zhang, B., Li, J., Guo, P., and Lv, Q., 2017. “Experimental studies on the effect of reynolds and weber numbers on the impact forces of low-speed droplets colliding with a solid surface”. *Experiments in Fluids*, **58**(9), p. 125.
- [32] Jonkman, J., and Musial, W., 2010. Offshore code comparison collaboration (oc3) for iea wind task 23 offshore wind technology and deployment. Tech. rep., National Renewable Energy Lab.(NREL), Golden, CO (United States).
- [33] Shirzadeh, R., Devriendt, C., Bidakhvidi, M. A., and Guillaume, P., 2013. “Experimental and computational damping estimation of an offshore wind turbine on a monopile foundation”. *Journal of Wind Engineering and Industrial Aerodynamics*, **120**, pp. 96–106.

- [34] Morison, J., Johnson, J., Schaaf, S., et al., 1950. “The force exerted by surface waves on piles”. *Journal of Petroleum Technology*, **2**(05), pp. 149–154.
- [35] Hasselmann, K., 1973. “Measurements of wind wave growth and swell decay during the joint north sea wave project (jonswap)”. *Deutschen Hydrografischen Zeitschrift*, **8**, p. 95.
- [36] Verma, A. S., Gao, Z., Jiang, Z., Ren, Z., and Vedvik, N. P., 2019. “Structural safety assessment of marine operations from a long-term perspective: A case study of offshore wind turbine blade installation”. In ASME 2019 38th International Conference on Ocean, Offshore and Arctic Engineering, American Society of Mechanical Engineers Digital Collection.
- [37] Madsen, H. A., Riziotis, V., Zahle, F., Hansen, M. O. L., Snel, H., Grasso, F., Larsen, T. J., Politis, E., and Rasmussen, F., 2012. “Blade element momentum modeling of inflow with shear in comparison with advanced model results”. *Wind Energy*, **15**(1), pp. 63–81.
- [38] Pirrung, G. R., Madsen, H. A., Kim, T., and Heinz, J., 2016. “A coupled near and far wake model for wind turbine aerodynamics”. *Wind Energy*, **19**(11), pp. 2053–2069.
- [39] Mann, J., 1994. “The spatial structure of neutral atmospheric surface-layer turbulence”. *Journal of Fluid Mechanics*, **273**, pp. 141–168.
- [40] Ren, Z., Skjetne, R., Verma, A. S., Jiang, Z., Gao, Z., and Halse, K. H. “Active heave compensation of floating wind turbine installation using a catamaran construction vessel”. *Marine Structures*, **75**, p. 102868.